Spatial Organization of Dps and DNA–Dps Complexes

Evgeniy V. Dubrovin[a,b*], Liubov A. Dadinova[c], Maxim V. Petoukhov[c], Ekaterina Yu. Soshinskaya[c], Andrey A. Mozhaev[c,d], Dmitry V. Klinov[e], Tilman E. Schäffer[f], Eleonora V. Shtykova[c], Oleg V. Batishchev[a]

[a]A.N. Frumkin Institute of Physical Chemistry and Electrochemistry, Russian Academy of Sciences, 31/4 Leninskiy prospekt, Moscow, 119071, Russia

[b]Lomonosov Moscow State University, Faculty of Physics, Leninskie Gory 1 bld 2, 119991, Moscow, Russia

[c]Shubnikov Institute of Crystallography, Federal Scientific Research Centre "Crystallography and Photonics," Russian Academy of Sciences, 119333, Moscow, Russia

[d]Shemyakin–Ovchinnikov Institute of Bioorganic Chemistry, Russian Academy of Sciences, 117997, Moscow, Russia

[e]Federal Research and Clinical Center of Physical-Chemical Medicine of Federal Medical Biological Agency, Malaya Pirogovskaya 1a, 119435, Moscow, Russia

[f]University of Tübingen, Institute of Applied Physics, Auf der Morgenstelle 10, 72076, Tübingen, Germany

*Corresponding author email:

dubrovin@polly.phys.msu.ru (Evgeniy V. Dubrovin)

Abstract

DNA co-crystallization with Dps family proteins is a fundamental mechanism, which preserves DNA in bacteria from harsh conditions. Though many aspects of this phenomenon are well characterized, the spatial organization of DNA in DNA–Dps co-crystals is not completely understood, and existing models need further clarification. To advance in this problem we have utilized atomic force microscopy (AFM) as the main structural tool, and small-angle X-scattering (SAXS) to characterize Dps as a key component of the DNA-protein complex. SAXS analysis in the presence of EDTA indicates a significantly larger radius of gyration for Dps than would be expected for the core of the dodecamer, consistent with the N-terminal regions extending out into solution and being accessible for interaction with DNA. In AFM experiments, both Dps protein molecules and DNA–Dps complexes adsorbed on mica or highly oriented pyrolytic graphite (HOPG) surfaces form densely packed hexagonal structures with a characteristic size of about 9 nm. To shed light on the peculiarities of DNA interaction with Dps molecules, we have characterized individual DNA–Dps complexes. Contour length evaluation has confirmed the non-specific character of Dps binding with DNA and revealed that DNA does not wrap Dps molecules in DNA–Dps complexes. Angle analysis has demonstrated that in DNA–Dps complexes a Dps molecule contacts with a DNA segment of ~6 nm in length. Consideration of DNA condensation upon complex formation with small Dps quasi-crystals indicates that DNA may be arranged along the rows of ordered protein molecules on a Dps sheet.

Keywords

Single-molecule analysis; DNA–Dps co-crystals; atomic force microscopy; DNA–protein interaction; small-angle X-scattering.

Introduction

During their lifecycle, many bacteria face harsh conditions such as oxidative cleavage [1], nucleases [2], UV and gamma irradiation, thermal stress, iron and copper toxicity, and acid and base shock [3]. To protect their genome from possible harmful effects, bacteria sequester DNA inside a cell by co-crystallization of DNA with a ferritin superfamily protein Dps (abbreviated from "DNA binding proteins from starved cells"), which is accumulated in bacterial cells during the stationary phase [4]. An *E.coli* Dps molecule consists of 12 identical subunits, each containing 167 amino acids and having a molecular weight of ~18.7 kDa [2]. High biological relevance of DNA–Dps co-crystals makes the detailed understanding of their spatial organization extremely important.

The effect of DNA co-crystallization with Dps has been extensively studied since its discovery in 1992 [2,5,6]. For the investigation of DNA–Dps co-crystals, transmission electron microscopy (TEM), fluorescence microscopy, X-ray crystallography, and small-angle X-ray scattering (SAXS) are generally used [7–14]. Both natural DNA–Dps co-crystals inside the cytoplasm of starved bacterial cells and model DNA–Dps co-crystals produced *in vitro* have been visualized using TEM and Cryo-EM [2,12,13,15], which showed that Dps binding with DNA was non-specific and mediated mainly by electrostatic interaction [2,14]. In particular, the disordered lysine-rich N-terminal region of *E.coli* Dps is responsible for electrostatic attraction with negatively charged DNA phosphate groups [16]. The SAXS technique was applied to determine the role and conformation of the N-terminal regions of the two types of Dps from *Deinococcus radiodurans* [17]. According to the results of this work one can conclude that when Dps is isolated from different organisms it has similar structural features necessary for DNA binding. However, members of the Dps family, which do not contain the positively charged N-terminal regions, cannot bind DNA [18–20].

It was demonstrated that Dps may co-crystallize with DNA of different lengths (from ~3000 to ~10000 base pairs) and nucleotide sequences [13]. Moreover, the crystallographic parameters of DNA–Dps co-crystals produced by closed supercoiled plasmids, linear double-stranded DNA and single-stranded RNA molecules are undistinguishable from those of pure Dps crystals: both form a tightly-packed, multilayered structure of hexagonally arranged Dps dodecamers with a spacing of ~7.8 nm, which corresponds to a unit cell of ~9 nm [15].

There are several hypothetical models for DNA spatial organization in DNA–Dps co-crystals. One of these models implies that DNA molecules are threaded through the holes in the hexagonal lattices of Dps dodecamers crossing different Dps sheets [21]. Another model assumes DNA wrapping around Dps molecules in a histone-like manner [22]. Moreover, several models suggest that DNA is accommodated in the grooves present in Dps dodecamer lattices and is aligned along the rows of Dps molecules within one Dps sheet [23,24]. Finally, there is a model that admits DNA accommodation both within one Dps sheet and across different Dps sheets [7]. The recent use of two complementary methods – small-angle X-ray scattering and cryo-electron tomography – obtained a detailed description of the structural organization of the DNA–Dps complex. It was demonstrated that cubic and triclinic structures were formed, depending on buffer parameters and local ion concentration, and the lattice parameters of the crystalline DNA–Dps complex were determined [12,13]. More importantly, and for the first time, DNA macromolecules in these co-crystals were visualized, although a mutual arrangement of DNA and Dps was different in the

various co-crystal structures [12,13]. In summarizing the above, one can conclude that the availability of the structural models of the co-crystals need additional validation or clarification.

Unique information about DNA–Dps co-crystal structure may be obtained from direct methods such as atomic force microscopy (AFM). AFM is a well-established tool for the investigation of individual DNA [25–27] and protein molecules [28,29], and DNA-protein complexes [30–34] with sub-nanometer spatial resolution. Unlike TEM, AFM renders operating in ambient conditions and aqueous environments, which are more relevant for biological specimens than vacuum. AFM has allowed the characterization of morphology and dimensions of the Dps containing nucleoid of lysed bacterial cells [10,11,35]. Moreover, AFM has revealed the varied ability of Dps family proteins to bind or condense DNA at a different pH [9,16,36,37] and showed certain Dps binding specificity towards DNA ends for short DNA fragments [38]. However, comprehensive and quantitative morphological analysis of individual DNA–Dps complexes and small quasi-crystals that may shed light on DNA arrangement in DNA–Dps co-crystals is still lacking.

The purpose of our study is to obtain evidence of DNA spatial organization in DNA–Dps co-crystals by AFM-based quantitative analysis of DNA bending and condensation upon complex formation with individual Dps molecules and small Dps quasi-crystals. In order to study single DNA–Dps complexes, we have used the previously elaborated approach for AFM investigation of individual DNA and protein molecules adsorbed on a highly oriented pyrolytic graphite (HOPG) surface modified with N,N'-(decane-1,10-diyl)bis(tetraglycineamide) (GM) [39–42]. SAXS reconstruction of a Dps molecule, including its N-terminal regions, was used to complement AFM data. The results contribute to the understanding of DNA compaction in DNA–Dps complexes and shed light on DNA organization in DNA–Dps co-crystals.

Materials and Methods

Materials

Freshly prepared Milli-Q water was used in the experiments, as well as two types of DNA plasmids. The circular vector pJET12-blunt 3130 bp was isolated as described in [43]. The mixture of pSPT18- and pSPT19-neo-DNA (~4500 bp each) cleaved with Eco RI (further referred to as linearized DNA) was obtained from Sigma-Aldrich (USA). Overexpression and purification of *E.coli* Dps was performed as described in [12]. A buffer containing 50 mM NaCl, 50 mM Tris-HCl and 0.5 mM EDTA (pH 8.0) was used for the preparation of DNA–Dps complexes and co-crystals, since it was shown to be most favorable for DNA–Dps co-crystallization [12].

Substrate preparation

A soaked mica surface was prepared by immersing a freshly cleaved (from both sides) muscovite mica slice in milli-Q water for 1 hour followed by drying in a stream of nitrogen. For HOPG modification, 10 µl of 0.01 mg/ml GM ($[Gly_4\text{-}NHCH_2]_2C_8H_{16}$, NanoTuning, Russia) solution in water was deposited onto a freshly cleaved HOPG surface (ZYB quality, mosaic spread 0.8−1.2°, NT-MDT, Russia) for 10 minutes, followed by drying in a stream of nitrogen.

Sample preparation for AFM

For AFM investigation of a Dps crystal, 50 µl of 70 µg/ml Dps solution in the buffer was deposited on a soaked mica surface prior to AFM imaging. For AFM investigation of individual Dps molecules, 1 µl of 2 µg/ml Dps solution in the buffer was deposited on a GM-HOPG surface for 3 seconds, followed by the addition of 40 µl of water and immediate drying in a stream of nitrogen.

For preparation of DNA–Dps co-crystals and DNA–Dps complexes we have used a Dps/DNA weight ratio of 5:1 according to the previous results [13]. For AFM investigation of DNA–Dps co-crystals, 7 μl of Dps solution (3.4 mg/ml) in the buffer was added to 2 μl of the circular plasmid DNA solution (2.6 mg/ml), and gently mixed and stored for 20 minutes at ~22°C. Then 50 μl of 5000 times buffer-diluted mixture was deposited on a soaked mica surface or a GM-HOPG surface prior to AFM imaging.

For AFM investigation of individual DNA–Dps complexes, 1.4 μl of Dps solution (0.9 mg/ml) in the buffer was added to 1 μl of the linearized plasmid DNA solution (0.25 mg/ml), and gently mixed and stored for 20 minutes at ~22°C. Afterwards, 0.5 μl of a 200 times buffer-diluted mixture was deposited on a GM-HOPG surface for 3 seconds, followed by the addition of 40 μl of water and immediate drying in a stream of nitrogen.

AFM imaging

AFM imaging of Dps crystals and DNA–Dps co-crystals was performed in the buffer solution in tapping mode on a Veeco Multimode atomic force microscope with a Nanoscope V controller (Veeco, USA) equipped with a tapping-mode fluid cell. For imaging we used silicon nitride triangular cantilevers SNL (A) (Bruker, USA) with a nominal spring constant of ~0.35 N/m (resonant frequency in water ~9 kHz). The scan rate was usually 1 Hz with 512 pixels × 512 pixels.

AFM imaging of the individual DNA and Dps molecules and DNA–Dps complexes was performed in an ambient environment in tapping mode on the MultiMode 8 atomic force microscope with a Nanoscope V controller (Bruker, USA). Silicon rectangular cantilevers PPP-NCHR (NanoWorld, Switzerland) with a nominal spring constant of ~42 N/m and a resonant frequency of 330 kHz were used. The scan rate was usually 1-2 Hz with 512×512 or 1024×1024 pixels.

Data processing

Femtoscan software (Advanced Technologies Center, Russia) [44] was used for AFM image processing, analysis (including characteristic size of hexagonal structures, height, volume, contour length and angle measurements) and presentation. The characteristic size of hexagonal structures was obtained by averaging diameters of Dps molecules measured in all three directions of protein ordering. The height of protein globules was measured manually as the difference between the level of the highest point on a globule and a substrate surface; AFM images with a pixel size no larger than 2 nm have been used for height analysis [45]. For contour length measurements, a DNA contour was rendered by a polyline (for DNA–Dps complexes a polyline was drawn through the center of Dps molecules). Standard deviation was used as an error value for height and length measurements.

For estimation of the lateral diameter of the Dps molecules we used the approach for AFM tip deconvolution of protein molecules in protein–DNA samples [46]. First, we estimated a tip radius (r_T = 6.4 ± 1.2 nm) from the AFM images of DNA molecules obtained with the same tip using a step-like model, in which the section of an object (DNA molecule in this case) is considered as a rectangle with the apparent height from the AFM images (0.89 ± 0.11 nm, N=20). Then, the same model was used to estimate the real (deconvoluted) lateral diameter (width) of adsorbed Dps molecules from the obtained value of r_T and the apparent width of Dps molecules.

Unpaired two-sample t-tests at a significance level 0.01 were applied for the assessment of statistical significance of mean height and width differences.

Angles θ between the tangents to a DNA contour for DNA–Dps complexes (Figure 5b, right central part) were measured manually using the corresponding tool in the software. The standard deviation of the mean was used as an error for $\langle\cos(\theta)\rangle$. Angle θ values for free DNA molecules have been calculated in Scilab 5.3.3 (https://www.scilab.org/) script, as described previously [47]. In brief, DNA contours were digitized, and angles θ between all pairs of points on a DNA molecule and separated by 22 nm along the contour with a step length of 22 nm were measured. The resulting histograms of the angle θ distribution were flipped over to zero to obtain the Gaussian fits ($y = A*\exp(-0.5*((x-x_c)/w)^2)$). For the estimation of the DNA contact length with a Dps molecule we neglected the relative error (standard deviation of the mean) for $\langle\cos(\theta)\rangle$ for free DNA molecules, as compared to that for DNA–Dps complexes, due to at least 10-times larger statistics for free DNA molecules.

For analysis of Dps binding specificity, the contour distance D_{end} between each Dps molecule in a DNA–Dps complex and its nearest end was divided by the contour length L of a complex. Such normalization of D_{end} allows the exclusion of systematic uncertainty associated with a uniform extension of DNA molecules adsorbed on a substrate.

SAXS reconstruction

Synchrotron SAXS experiments were performed at the European Molecular Biology Laboratory (EMBL) on the EMBL-P12 BioSAXS beam line at the PETRAIII storage ring (DESY, Hamburg) [48].

The Dps protein was expressed and purified as described in [12]. A buffer containing 50 mM NaCl, 50 mM Tris-HCl, and 0.5 mM EDTA (pH 8.0) was used for SAXS measurements in solution. Since no concentration dependence was observed, structural characteristics of the Dps protein were studied at a concentration of 3.5 mg/ml.

Radii of gyration R_g were calculated from the initial part of the scattering curve in the lowest s region using the following equation:

$$I_{\exp}(s) = I(0)\exp(-s^2R_g^2/3), \quad (1)$$

that is valid in the range $(sR_g) < 1.3$.

Distance distribution function, $p(r)$ was computed by the GNOM program [49] using the equation

$$p(r) = \frac{1}{2\pi^2}\int_0^\infty s\, r\, I(s)\, sin(sr)ds, \quad (2)$$

where $I(s)$ is the scattering intensity, $s = (4\pi\sin\theta)/\lambda$ is the scattering vector, 2θ is the scattering angle, and $\lambda = 0.124$ nm is the scattering wavelength. The maximum particle size (D_{max}) was determined from the condition $p(r) = 0$ at $r > D_{max}$. SAXS analysis and model fitting were performed in the most informative part of the range of the scattering curve $0.08 < s < 2.1$ nm^{-1}. The low-resolution shapes of the full-length Dps protein were reconstructed ab initio from the $p(r)$ function using an *ab initio* procedure and the DAMMIN program [50]. The program utilizes a simulated annealing algorithm to build models fitting the experimental data $I_{exp}(s)$ to minimize the discrepancy

$$\chi^2 = \frac{1}{N-1}\sum_j\left[\frac{I_{exp}(s_j) - c\, I_{calc}(s_j)}{\sigma(s_j)}\right]^2, \quad (3)$$

i.e., the reduced χ^2 test, where N is the number of experimental points, c is a scaling factor and $I_{calc}(s_j)$ and $\sigma(s_j)$ are the calculated intensity from the model and the experimental error of the momentum transfer s_j, respectively.

The reconstruction of the protein structure and the structures of flexible N-terminal fragments, which are absent in the crystallographic structure of the Dps protein, was performed using a hybrid method and the CORAL program [51], which combines an *ab initio* algorithm and rigid-body modeling. The program utilizes high-resolution structures from the Protein Data Bank and the theoretical intensities calculated by the CRYSOL program [52], and adds fragments of the macromolecule missing in the high-resolution model by using an *ab initio* procedure. The atomic-resolution structure of the Dps protein (PDB ID: 1DPS) was used for the hybrid modeling.

The ensemble optimization method (EOM) [53,54] was applied to assess the flexibility of the N-terminal fragments of Dps. In essence, EOM consists of two stages: first, a large pool of models (~10000) is generated where the potentially flexible parts (linkers and disordered terminal regions) are taken as random chains. Second, a genetic algorithm (GA) is employed to select an optimized sub-ensemble such that the averaged scattering curve from these models fits the experimental SAXS data. A comparison of the obtained distribution of structural descriptors such as maximal size D_{max} and radius of gyration R_g in the selected models, with the corresponding distributions in the original pool, provides information about the flexibility, disorder and degree of extension. More precisely, the position and width of the resulting distribution ascertains whether the disordered part is compact or spread, and possesses the monomodal or multimodal conformation.

The protein models reconstructed by different methods were analyzed with the SUPCOMB program [55] to determine the dissimilarity in their structural organization and find the normalized spatial discrepancies (NSD).

Results and Discussion

SAXS reconstruction of the Dps structure in solution

Since it is known that the structure of the Dps protein, particularly the conformation of its N-terminal regions, is essential for the protective co-crystallization with DNA [16,17], a preliminary study of the protein structure was undertaken using SAXS. Interactions with negatively charged bases of DNA occur through positively charged lysines (Lys_5, Lys_8, and Lys_{10}) and arginine (Arg_{18}) located in the N-terminal fragments of Dps from *E.coli*. Thus, the three-dimensional location and accessibility of these amino acids for DNA are of great importance, and the aim of this preliminary study was to demonstrate protein readiness for the complex formation.

The SAXS profile for the Dps protein in solution and the corresponding distance distribution function $p(r)$ are presented in Figure 1a.

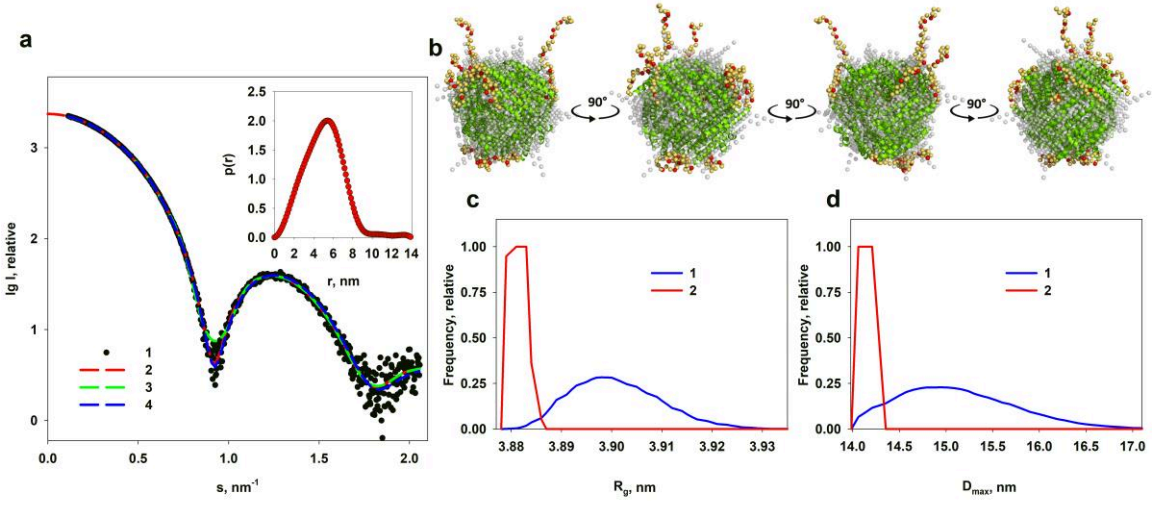

Figure 1. (a): The experimental scattering curve of the Dps protein (1), the simulated curves calculated from the distance distribution function *p(r)* (2), DAMMIN model (3), and CORAL model (4). Inset: the distance distribution function *p(r)*. (b) The superposition of the DAMMIN model (gray spheres) and the CORAL model demonstrated in 4 different orientations for better visualization: green helices – the high-resolution structure of the Dps protein (PDB ID: 1DPS) and yellow spheres – reconstructed N-terminal regions. The residues Lys_5, Lys_8, Lys_{10}, and Arg_{18} are represented by red spheres in the CORAL model. (c) & (d) EOM analysis: R_g and D_{max} distributions, respectively. Red lines are the selected ensembles, and blue lines are the original pools of 10000 random conformations.

Twelve disordered N-domains contribute to the scattering of the full-length protein in solution; however, this contribution is rather small: distance distribution function *p(r)* in the region close to the maximum size D_{max} shows low *p(r)* amplitude due to low electron density of the N-terminal regions (Fig 1a, inset). Nonetheless, scattering from these regions leads to an increase of the maximal size of the protein up to 14 nm, as compared to the protein core with the size of about 9 nm. *Ab initio* shape reconstruction of the Dps protein was carried out using the *p(r)* function and the DAMMIN program. Since the protein exists in solution as a dodecamer, symmetry *P*23 was applied. The *ab initio* method of shape restoration does not consider the localization of the disordered N-termini, thus, to ensure their relatively uniform arrangement on the dodecamer surface it was necessary to introduce the symmetry. Otherwise, to fit the experimental scattering curve and to match the calculated radius of gyration R_g = 3.9±0.1 nm and maximum size D_{max} = 14 nm, the DAMMIN program would have to create a model consisting of a spherical core, as the main scattering part of the protein and a single long "tail". The reconstructed symmetrical model demonstrates a hollow spherical shape with a diameter of about 9 nm and protruding parts, which apparently belong to the N-terminal regions of the protein (Fig 1b). This relatively rough model of low-resolution yields is, nevertheless, a reasonable fit to the experimental SAXS data (χ^2 = 1.9).

To determine a more accurate, full-length structure of the protein and a configuration of its N-terminal fragments, the hybrid approach implemented in the CORAL program was employed. The full-length structure of the protein was modeled using atomic coordinates of the high resolution Dps structure (PDB ID: 1DPS), and the *ab initio* algorithm for the reconstruction of the first N-terminal 22 amino acid residues of the protein missing in the crystal lattice. The reconstructed model displayed in Fig 1b shows flexible N-terminal regions of the proteins freely extended into solution. More importantly, residues Lys_5, Lys_8, Lys_{10}, and Arg_{18}, represented by red spheres in the CORAL model, are quite accessible for interaction with DNA. The discrepancy χ^2 for this reconstruction is 1.1, i.e., the scattering from the model is in very good agreement with the experimental data.

It should also be noted here that the protein core without N-termini obtained by the *ab initio* procedure (the DAMMIN program) and by the hybrid approach (CORAL program using Dps crystal structure) coincide. The quantitative mutual agreement between the reconstruction of the Dps structure by two methods was evaluated by the SUPCOMB program. The normalized spatial discrepancy (NSD) was 1.6, i.e., two independent approaches to the modeling giving similar results.

The model of full-length Dps obtained by the CORAL program demonstrates that the disordered N-termini of different chains of the dodecamer have both extended and more compact conformations (Fig 1b). To analyze the unfolding and flexibility of the disordered N-termini of the protein, the EOM approach was employed. The conformation of one loop from the Dps monomer was sampled while all other chains were kept in the original configuration, as in the initial CORAL model. The optimized ensemble obtained by EOM points mainly to the disordered regions located closer to the

surface of the dodecamer. Both R_g and D_{max} distributions (in Fig 1c & d) of the selected ensemble demonstrate smaller values when compared to the original pool of 10000 random conformations. This indicates that despite the disordering not all 12 N-terminal loops can simultaneously protrude far from the surface of the Dps protein. The observed extended and compact conformations of the N-termini are in dynamic equilibrium in solution, and, therefore, each of them can provide interaction with DNA.

More important, only in the presence of EDTA in the buffer composition, as used in this work, the disordered N-termini can freely extend into solution and the residues Lys_5, Lys_8, Lys_{10}, and Arg_{18}, represented as red spheres in Fig 1b, are accessible for interaction with DNA. Whereas, in the EDTA-free buffer, all disordered N-domains are located closer to the protein surface, and no DNA–Dps crystalline complex can be obtained [56]. As a chelating agent EDTA weakens interaction between iron and amino acids of Dps facilitating unfolding of a Dps N-terminal region and its interactions with DNA. Consequently the conformation of Dps N-terminal regions in the presence of EDTA becomes more flexible and extended. The corresponding protein structures are deposited in the Small Angle Scattering Biological Data Bank (SASBDB; https://www.sasbdb.org/) with SASBDB Accession Codes: SASDKF4 for Dps in solution in the presence of EDTA, and SASDKY4 for Dps in the EDTA-free buffer.

Therefore, it should be concluded that the SAXS reconstruction of Dps has revealed that the N-terminal regions of the proteins are accessible for interaction with DNA. DNA–Dps complexes were a subject of further analysis with AFM.

Surfaces of arranged Dps molecules and DNA–Dps complexes

The AFM image of a Dps crystal surface obtained in buffer solution on a soaked mica surface is presented in Figure 2a. It confirms what is already known from the TEM measurements: Dps molecules arrange into a two-dimensional crystal structure with a three-fold symmetry (an enlarged region of the AFM image and its Fourier transform are presented on the right). The characteristic size of the Dps crystal surface, 9.2 ± 0.3 nm (N=100), is in agreement with the previous reports [15] and corresponds well to the diameter of the Dps molecule, known from its crystallographic structure (~9 nm [21]).

A typical AFM image of DNA–Dps complexes deposited on a soaked mica surface is shown in Figure 2b. DNA–Dps complexes also form a hexagonal pattern (an enlarged region of the AFM image and its Fourier transform are presented on the right); the characteristic size of the hexagonal packing, 9.10 ± 0.24 nm (N=100), corresponds within an error to that of a Dps crystal (Figure 2a). Since there is no evidence that the AFM tip touches the substrate surface in the defects in the hexagonal pattern of Dps molecules (darker regions in Figure 2a & b), the height of the layer cannot be determined from these images. However, the height of the 2D DNA–Dps co-crystal has been measured from the relatively small fragments of DNA–Dps co-crystal formed on a GM-HOPG surface (Figure 2c). The height of the crystal is ~ 9 nm (Figure 2d), which corresponds to the crystallographic diameter of a Dps molecule [21].

The structure and dimensions of the unit cell of a Dps crystal, and a DNA–Dps co-crystal observed in AFM images, are in agreement with TEM data [15]. AFM operating in tapping mode in aqueous solutions is capable to image even loosely physisorbed and thermally moving DNA molecules [25]. However, DNA molecules are not discerned in the AFM images (Figure 2b), indicating that they may be located between or beneath the arranged Dps molecules and are not accessible to the AFM tip.

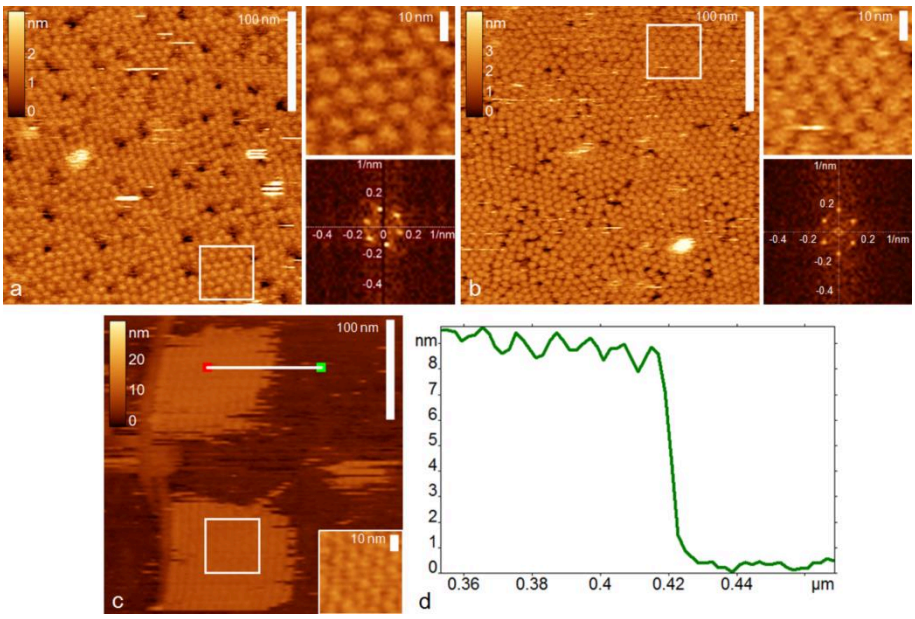

Figure 2. (a, b) AFM images of (a) Dps molecules and (b) DNA–Dps complexes adsorbed on a soaked mica in a buffer solution. The regions in the box are enlarged at the top right. Fourier transformations of the enlarged regions are shown at the bottom right. (c) AFM image of DNA–Dps complexes adsorbed on a GM-HOPG surface in a buffer solution. (d) Height profile along the horizontal line in the AFM image. The AFM images were obtained in the buffer solution. The sizes of the AFM images are 300×300 nm^2 (enlarged regions – 50×50 nm^2).

Individual Dps molecules and DNA–Dps complexes

To explore the DNA spatial arrangement in DNA–Dps complexes, we have visualized and characterized the morphology of individual Dps molecules, DNA molecules and DNA–Dps complexes. For this purpose, we have decreased the concentration of the components in the DNA–Dps mixture by ~5 times, retaining the Dps/DNA ratio (see Experimental section). For the investigation of biomolecules, we deposited them onto a GM-HOPG surface. This surface has been shown to "trap" DNA molecules electrostatically at a low ionic strength [57], while retaining a native-like conformation of adsorbed globular proteins (including ferritin) after their deposition, followed by drying [39,58].

A typical AFM image of individual Dps molecules adsorbed onto a GM-HOPG surface is shown in Figure 3a. The dark spots on the surface correspond to the defects of a GM-layer; their depth is around 0.4 nm [59]. The molecules appear as globules with a mean height of 5.2 ± 0.4 nm (N=235; the height distribution histogram is shown in Figure 3b). The height value of a Dps molecule is smaller than its crystallographic diameter, probably due to protein deformation by the AFM tip [60], local probe-sample geometry [61], and protein dehydration. A wider tail of the height distribution towards smaller values may indicate the presence of the fraction of Dps molecules, which have not completely assembled into dodecamers, e.g., trimers [62]. The width of the Dps molecules that takes into account an AFM tip deconvolution (see Materials and Methods) is (8.1 ± 2.2) nm.

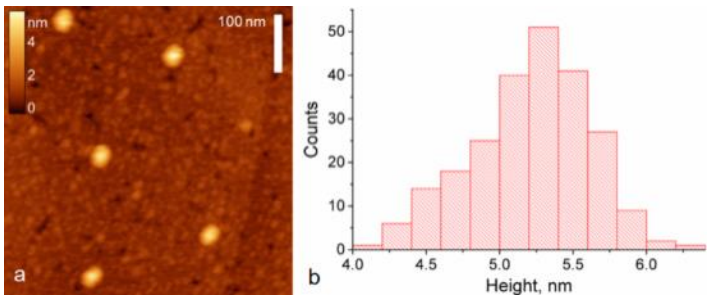

Figure 3. (a) AFM image and (b) height distribution of individual Dps molecules adsorbed on a GM-HOPG surface (the distribution is obtained from the analysis of several AFM images). The AFM image was obtained in air. The size of the AFM image is 500×500 nm^2.

The ability of superhelical circular plasmids to form melted (open) regions [63] and hairpin structures [64] may impede an accurate determination of the DNA contour length from AFM images (see also Supplemental Information, Figure S1). Thus, for the AFM investigation of individual DNA–Dps complexes, we have used linearized DNA plasmids. AFM images of the diluted mixture of the linearized DNA and Dps molecules deposited on a GM-HOPG surface, reveal individual DNA molecules containing 1 to 7 globules along their contour (representative examples are presented in Figure 4a; the upper left image shows a free linearized DNA molecule). The height distribution of these globules is shown in Figure 4b: their height (5.4 ± 0.3 nm, *N*=140) is similar to that of free Dps molecules adsorbed on a GM-HOPG surface (Figure 3). Therefore, we interpret the structures with globules in Figure 4a as individual DNA–Dps complexes.

The estimation of the real (deconvoluted) width of the Dps molecules DNA–Dps complexes gives (9.0 ± 2.2) nm. The morphological parameters (height, measured and deconvoluted width) of individual Dps molecules adsorbed on a GM-HOPG surface are summarized in Table 1. The height and width of Dps molecules within complexes are slightly larger than the values for free Dps molecules (Table 1); however, each of these differences is statistically significant (two sample t-test, p=0.01). The increase of the size (especially width) of Dps molecules in DNA–Dps complexes may be induced by the contact of a protein molecule with a DNA strand.

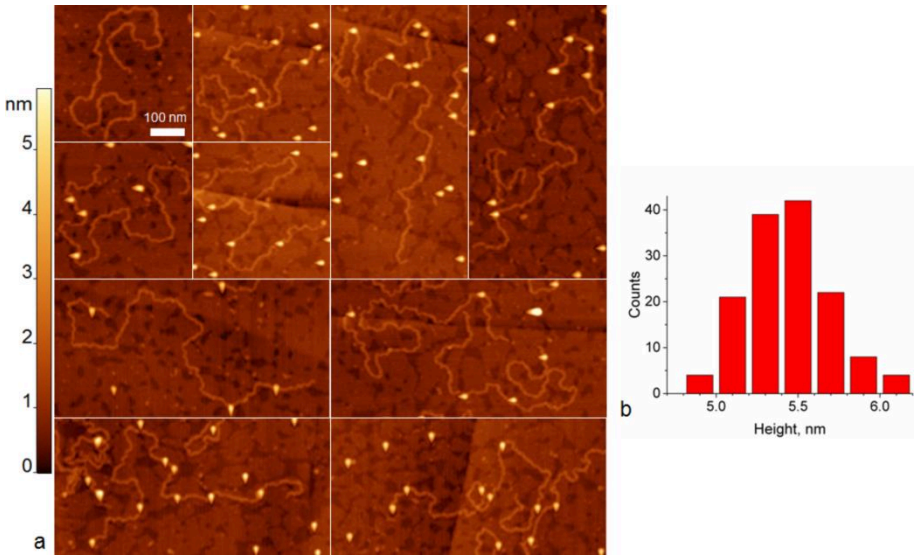

Figure 4. (a) A montage of AFM images of (upper left) a linearized DNA molecule and (other images) individual linearized DNA–Dps complexes adsorbed onto a GM-HOPG surface. The AFM images were obtained in air. The sizes of the AFM images are 400×400 nm^2, 400×800 nm^2 and 800×400 nm^2. (b) Height distribution of Dps molecules in the complexes.

Table 1. Morphological parameters (mean values ± SD, nm) of Dps molecules adsorbed on a GM-HOPG surface. N – number of measurements.

	Height	Width (measured)	Width (deconvoluted)
Free Dps molecules	5.2 ± 0.4 (N = 235)	21 ± 1 (N = 102)	8.1 ± 2.2
Dps molecules in DNA–Dps complexes	5.4 ± 0.3 (N = 140)	22 ±1 (N = 48)	9.0 ± 2.3

Analysis of contour length of DNA–Dps complexes

The mean contour lengths of free DNA molecules and DNA–Dps complexes containing 1 to 7 Dps molecules are within the range of 1500 – 1550 nm (Figure 5a). These values do not depend (within the errors) on the number of protein molecules bound to the DNA, which indicates that the DNA molecule does not wrap around the Dps molecule upon complex formation. This behavior differentiates Dps from histone proteins, which typically wrap around DNA [65]. However, these data do not exclude the fact that DNA may sweep along a Dps molecule. The previous work [13] demonstrated a parallel shift of the protein layers relative to each other, forming grooves for DNA accommodation, whereas DNA does not wrap around the protein, it only bends near it.

Analysis of DNA bending in DNA–Dps complexes

Information concerning DNA bending upon its binding with Dps molecules can be obtained from AFM images by directly measuring the angle θ between two tangents to the DNA contour at the entrance points of a protein globule (tangent method, Figure 5b, right central part) [66].

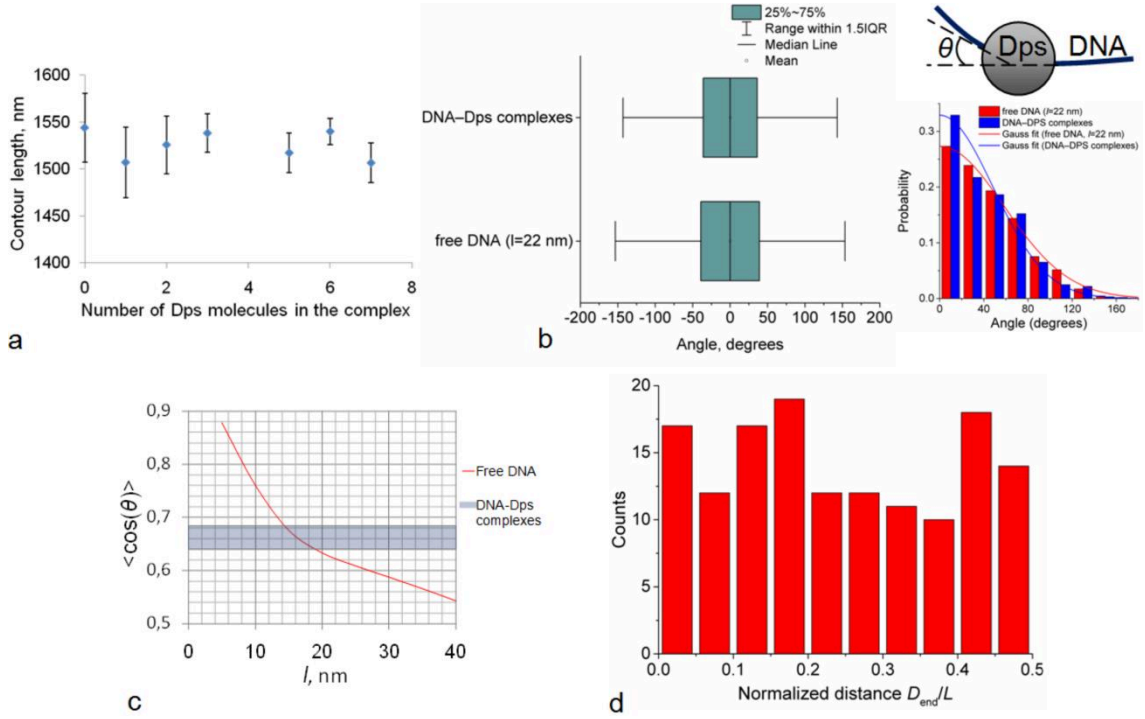

Figure 5. (a) Mean DNA–Dps complex length as a function of the number of bound molecules in the complex. (b) (left) Box chart for the distributions of the apparent DNA bending angle θ in DNA–Dps complexes and free DNA molecules at a contour distance l=22 nm flipped over a zero value; (bottom right) the corresponding distributions (solid lines are Gaussian fits for each distribution); (top right) the schematic illustrating the definition of the bending angle θ. (c) <cos(θ)> as a function of the contour length l of a segment of a free DNA molecule (thin red curve) and the value of <cos(θ)> for DNA–Dps complexes (grey line, the width takes into account the standard deviation of the mean). (d) Distribution of the normalized contour distance D_{end}/L between a Dps molecule in a DNA–Dps complex and its nearest end.

The distribution (and the box chart) of the angle θ for DNA–Dps complexes and its Gaussian fit are shown in Figure 5b with blue columns (the total number of analyzed complexes is 328) and a blue line, respectively. The maximum at a zero value may indicate that upon binding with DNA, Dps does not bend DNA. The length of a hidden DNA segment between two exit points of DNA arms coming out from a Dps molecule in AFM images can be estimated by an apparent (i.e., convoluted by an AFM tip) lateral diameter of a Dps molecule (22 ± 1 nm, Table 1). The distribution (and the box chart) of the angle θ for free DNA molecules obtained for a separation length of 22 nm is shown as a reference in Figure 5b with red columns (the total number of analyzed angles is 1515). The Gaussian fit of the distribution is shown with a red line. The observed differences in the angle distributions for DNA–Dps complexes and free DNA molecules may be caused by "freezing" the fluctuations of DNA contour orientation inside a certain DNA segment with a length l_{fix}, so that θ=0 at l_{fix}. The length of this segment may be considered as a contact length of DNA with a bound Dps molecule.

To estimate l_{fix} we have calculated <cos(θ)> for DNA–Dps complexes (0.662 ± 0.022 rad) and compared it with the dependence of <cos(θ)> on a segment length l for a free DNA molecule (Figure 5c). According to this graph, the length of the fluctuating DNA segment inside a broadened image of a Dps molecule is 16 ± 2 nm, which gives 6.0 ± 2.2 nm for the estimation of l_{fix}. Therefore, we can conclude that a DNA-bound Dps molecule contacts with a DNA segment of about 6 nm length.

Analysis of Dps binding specificity

To analyze the specificity of Dps binding with DNA, we have measured the contour distance D_{end} between each DNA bound Dps molecule and the nearest end of a complex (the total number of analyzed complexes was 143) [66]. The normalized distance D_{end}/L is rather evenly distributed along the DNA matrix (Figure 5d), indicating that the linearized plasmid DNA does not have pronounced Dps binding sites. This observation is in agreement with previous work reporting the absence of sequence specificity of Dps binding with DNA and the major role of electrostatic interactions in DNA–Dps binding [2,14]. The non-specific character of DNA–Dps binding justifies the utilization of linear DNA scaffolds to delineate the general characteristics of DNA–Dps complexes.

Analysis of DNA organization in DNA–Dps quasi-crystal formations

Moreover, some fractions of DNA–Dps complexes contain arrangements composed of several tens of Dps molecules (Figure 6a) ordered in a two-dimensional quasi-crystal structure (see the enlarged height and phase images in the middle and right columns, respectively). We suggest that spatial organization of DNA in these formations is similar to that in DNA–Dps co-crystals.

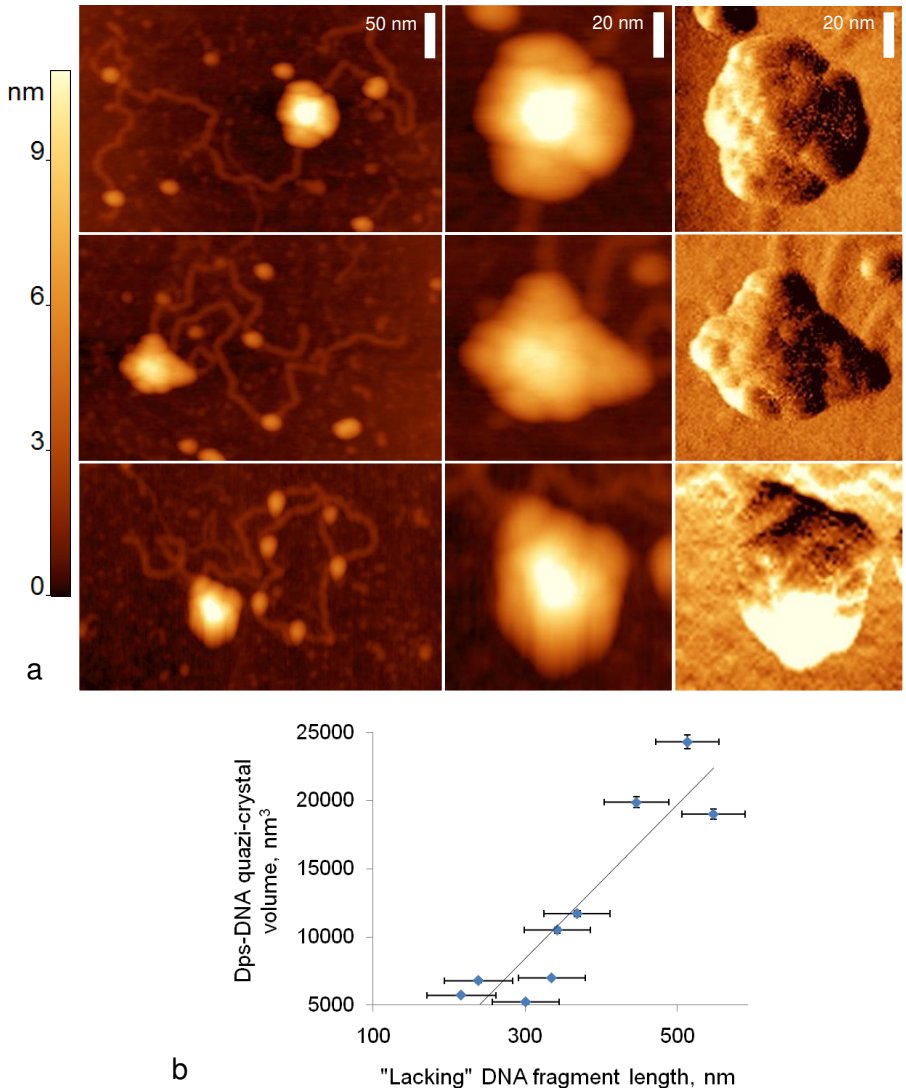

Figure 6. DNA spatial arrangement in DNA–Dps crystals. (a) (left column) A montage of AFM height images demonstrating individual complexes of plasmid DNA with small Dps arrangements (quasi-crystals). Enlarged regions with Dps arrangements are shown as height (middle column) and phase (right column). The

AFM images were obtained in air. The size of AFM images is 250×400 nm^2 (enlarged regions – 100×100 nm^2). (b) Volume of a of Dps-DNA quasi-crystals as a function of contour length of a "lacking" DNA fragment ($<L> - L_{vis.}$). A line of equality, i.e., having a slope angle of 45° is shown as a reference.

It is noteworthy that the cumulative contour length of each DNA–Dps complex outside the Dps arrangement (Figure 6a) is considerably (200 – 600 nm) smaller than the mean contour length of a DNA molecule, or DNA–Dps complexes containing 1 – 7 single Dps molecules (~1500 nm; Figure 5a). This observation provides an insight into DNA organization in a DNA–Dps co-crystal.

The observed decrease of the apparent contour length of DNA–Dps complexes can be assigned to a fraction of a DNA contour located inside the Dps arrangements of corresponding DNA–Dps complexes and therefore is not resolved in the AFM images. However, this "lacking" DNA fragment is always considerably larger than the lateral size of Dps arrangements, which is usually ~50 – 70 nm (Figure 6a). Therefore, the DNA contour cannot directly follow along a Dps arrangement from one entrance point of an apparent DNA contour to another. As discussed above (Figure 5a), DNA wrapping around Dps molecules is also unlikely and can be ruled out (except the outermost molecules in the protein arrangement). In light of these considerations, it follows that a DNA contour changes its direction several times inside a Dps arrangement. A radius of a Dps molecule (4.5 nm) is sufficient to allow DNA to turn without disruption of its helical structure (the threshold radius of DNA curvature is 3.5 nm [67]).

The volume of Dps-DNA quasi-crystals demonstrates a growth upon increase of the "lacking" DNA segment length ($<L> - L_{vis.}$, where $<L>$ is the mean DNA contour length and $L_{vis.}$ is the length of a visible fraction of a DNA contour in a DNA–Dps complex, Figure 6b). The linear fit of this dependence (shown with a line in Figure 6b) gives the coefficient of proportionality between the volume and the length of 56±9 nm^2 (R^2=0.83). Considering an apparent volume (i.e. a volume including all spaces between a molecule and a substrate) of one Dps molecule in a Dps-DNA co-crystal as a volume of a rectangular parallelepiped with 9×9 nm base and 5.2±0.4 nm height (Table 1), we can estimate the length of a DNA per one Dps molecule in a Dps-DNA quasi-crystal as 7.5±1.4 nm. This value corresponds to a ~7.8 nm spacing of hexagonally arranged Dps dodecamers.

The obtained estimation fits very well the model proposed in [13] from the results of small-angle X-ray scattering data. According to this model, the contour of a DNA molecule follows along the rows of ordered Dps molecules in a hexagonal Dps sheet. The model is insensitive to the particular DNA path and only defines a general organization of DNA relative to Dps molecules in the crystal. In complexes such as those in Figure 6a, a DNA thread may turn around when it reaches the boundary of a Dps arrangement.

Conclusions

The obtained SAXS reconstruction of Dps molecules have shown that the N-terminal regions of the protein freely extend into solution and are accessible for interaction with DNA. Using linearized plasmids as a model DNA scaffold, we have visualized and characterized individual DNA–Dps complexes with sub-molecular resolution. The analysis of contour lengths of DNA complexes with single Dps molecules has demonstrated that DNA does not wrap around Dps molecules upon complex formation, ruling out a histone-like organization of DNA in DNA–Dps complexes. Tangent method analysis has demonstrated that Dps molecules contact with a ~6 nm DNA segment

in the vicinity of a binding site. Moreover, AFM does not reveal specific binding of Dps to the plasmid DNA molecule. The analysis of contour lengths of individual DNA complexes with small Dps quasi-crystals evidences that DNA may be arranged along the rows of ordered Dps molecules in a sheet of a Dps crystal.

Acknowledgements

The work was supported by the Ministry of Science and Higher Education of the Russian Federation (project # AAAA-A20-120101090002-4) in part of AFM study. SAXS analysis and providing samples were supported by the Russian Science Foundation (project no. 18-74-10071).

References

[1] A. Martinez, R. Kolter, Protection of DNA during oxidative stress by the nonspecific DNA-binding protein Dps., Journal of Bacteriology. 179 (1997) 5188–5194. https://doi.org/10.1128/jb.179.16.5188-5194.1997.

[2] M. Almirón, A.J. Link, D. Furlong, R. Kolter, A novel DNA-binding protein with regulatory and protective roles in starved Escherichia coli., Genes Dev. 6 (1992) 2646–2654. https://doi.org/10.1101/gad.6.12b.2646.

[3] S. Nair, S.E. Finkel, Dps Protects Cells against Multiple Stresses during Stationary Phase, Journal of Bacteriology. 186 (2004) 4192–4198. https://doi.org/10.1128/JB.186.13.4192-4198.2004.

[4] S. Stefanini, P. Ceci, M. Ardini, A. Ilari, DNA-Binding Proteins From Starved Cells (Dps Proteins), in: Handbook of Metalloproteins, American Cancer Society, 2010. https://doi.org/10.1002/0470028637.met258.

[5] Z. Reich, E.J. Wachtel, A. Minsky, Liquid-crystalline mesophases of plasmid DNA in bacteria, Science. 264 (1994) 1460–1463. https://doi.org/10.1126/science.8197460.

[6] D. Frenkiel-Krispin, I. Ben-Avraham, J. Englander, E. Shimoni, S.G. Wolf, A. Minsky, Nucleoid restructuring in stationary-state bacteria, Molecular Microbiology. 51 (2004) 395–405. https://doi.org/10.1046/j.1365-2958.2003.03855.x.

[7] A. Moiseenko, N. Loiko, K. Tereshkina, Y. Danilova, V. Kovalenko, O. Chertkov, A.V. Feofanov, Y.F. Krupyanskii, O.S. Sokolova, Projection structures reveal the position of the DNA within DNA-Dps Co-crystals, Biochemical and Biophysical Research Communications. 517 (2019) 463–469. https://doi.org/10.1016/j.bbrc.2019.07.103.

[8] Y.T. Sato, S. Watanabe, T. Kenmotsu, M. Ichikawa, Y. Yoshikawa, J. Teramoto, T. Imanaka, A. Ishihama, K. Yoshikawa, Structural Change of DNA Induced by Nucleoid Proteins: Growth Phase-Specific Fis and Stationary Phase-Specific Dps, Biophysical Journal. 105 (2013) 1037–1044. https://doi.org/10.1016/j.bpj.2013.07.025.

[9] P. Ceci, L. Mangiarotti, C. Rivetti, E. Chiancone, The neutrophil-activating Dps protein of Helicobacter pylori, HP-NAP, adopts a mechanism different from Escherichia coli Dps to bind and condense DNA, Nucleic Acids Res. 35 (2007) 2247–2256. https://doi.org/10.1093/nar/gkm077.

[10] K. Morikawa, R.L. Ohniwa, J. Kim, S.L. Takeshita, A. Maruyama, Y. Inose, K. Takeyasu, T. Ohta, Biochemical, Molecular Genetic, and Structural Analyses of the Staphylococcal Nucleoid, Microscopy and Microanalysis. 13 (2007) 30–35. https://doi.org/10.1017/S1431927607070080.

[11] J. Kim, S.H. Yoshimura, K. Hizume, R.L. Ohniwa, A. Ishihama, K. Takeyasu, Fundamental structural units of the Escherichia coli nucleoid revealed by atomic force microscopy, Nucleic Acids Res. 32 (2004) 1982–1992. https://doi.org/10.1093/nar/gkh512.

[12] R. Kamyshinsky, Y. Chesnokov, L. Dadinova, A. Mozhaev, I. Orlov, M. Petoukhov, A. Orekhov, E. Shtykova, A. Vasiliev, Polymorphic Protective Dps–DNA Co-Crystals by Cryo Electron Tomography and Small Angle X-Ray Scattering, Biomolecules. 10 (2020) 39. https://doi.org/10.3390/biom10010039.

[13] L.A. Dadinova, Y.M. Chesnokov, R.A. Kamyshinsky, I.A. Orlov, M.V. Petoukhov, A.A. Mozhaev, E.Y. Soshinskaya, V.N. Lazarev, V.A. Manuvera, A.S. Orekhov, A.L. Vasiliev,

E.V. Shtykova, Protective Dps–DNA co-crystallization in stressed cells: an in vitro structural study by small-angle X-ray scattering and cryo-electron tomography, FEBS Letters. 593 (2019) 1360–1371. https://doi.org/10.1002/1873-3468.13439.
[14] D. Frenkiel-Krispin, S. Levin-Zaidman, E. Shimoni, S.G. Wolf, E.J. Wachtel, T. Arad, S.E. Finkel, R. Kolter, A. Minsky, Regulated phase transitions of bacterial chromatin: a non-enzymatic pathway for generic DNA protection, The EMBO Journal. 20 (2001) 1184–1191. https://doi.org/10.1093/emboj/20.5.1184.
[15] S.G. Wolf, D. Frenkiel, T. Arad, S.E. Finkel, R. Kolter, A. Minsky, DNA protection by stress-induced biocrystallization, Nature. 400 (1999) 83–85. https://doi.org/10.1038/21918.
[16] P. Ceci, S. Cellai, E. Falvo, C. Rivetti, G.L. Rossi, E. Chiancone, DNA condensation and self-aggregation of Escherichia coli Dps are coupled phenomena related to the properties of the N-terminus, Nucleic Acids Res. 32 (2004) 5935–5944. https://doi.org/10.1093/nar/gkh915.
[17] S.P. Santos, M.G. Cuypers, A. Round, S. Finet, T. Narayanan, E.P. Mitchell, C.V. Romão, SAXS Structural Studies of Dps from Deinococcus radiodurans Highlights the Conformation of the Mobile N-Terminal Extensions, Journal of Molecular Biology. 429 (2017) 667–687. https://doi.org/10.1016/j.jmb.2017.01.008.
[18] M. Bozzi, G. Mignogna, S. Stefanini, D. Barra, C. Longhi, P. Valenti, E. Chiancone, A Novel Non-heme Iron-binding Ferritin Related to the DNA-binding Proteins of the Dps Family in Listeria innocua, J. Biol. Chem. 272 (1997) 3259–3265. https://doi.org/10.1074/jbc.272.6.3259.
[19] E. Papinutto, W.G. Dundon, N. Pitulis, R. Battistutta, C. Montecucco, G. Zanotti, Structure of Two Iron-binding Proteins from Bacillus anthracis, J. Biol. Chem. 277 (2002) 15093–15098. https://doi.org/10.1074/jbc.M112378200.
[20] G. Zanotti, E. Papinutto, W.G. Dundon, R. Battistutta, M. Seveso, G.D. Giudice, R. Rappuoli, C. Montecucco, Structure of the Neutrophil-activating Protein from Helicobacter pylori, Journal of Molecular Biology. 323 (2002) 125–130. https://doi.org/10.1016/S0022-2836(02)00879-3.
[21] R.A. Grant, D.J. Filman, S.E. Finkel, R. Kolter, J.M. Hogle, The crystal structure of Dps, a ferritin homolog that binds and protects DNA, Nature Structural Biology. 5 (1998) 294–303. https://doi.org/10.1038/nsb0498-294.
[22] K. Zeth, Dps biomineralizing proteins: multifunctional architects of nature, Biochem J. 445 (2012) 297–311. https://doi.org/10.1042/BJ20120514.
[23] A. Minsky, E. Shimoni, D. Frenkiel-Krispin, Stress, order and survival, Nature Reviews Molecular Cell Biology. 3 (2002) 50–60. https://doi.org/10.1038/nrm700.
[24] B. Ren, G. Tibbelin, T. Kajino, O. Asami, R. Ladenstein, The Multi-layered Structure of Dps with a Novel Di-nuclear Ferroxidase Center, Journal of Molecular Biology. 329 (2003) 467–477. https://doi.org/10.1016/S0022-2836(03)00466-2.
[25] E.V. Dubrovin, M. Schächtele, T.E. Schäffer, Nanotemplate-directed DNA segmental thermal motion, RSC Adv. 6 (2016) 79584–79592. https://doi.org/10.1039/C6RA14383K.
[26] D. Murugesapillai, S. Bouaziz, L. James Maher, N. E. Israeloff, C. E. Cameron, M. C. Williams, Accurate nanoscale flexibility measurement of DNA and DNA–protein complexes by atomic force microscopy in liquid, Nanoscale. 9 (2017) 11327–11337. https://doi.org/10.1039/C7NR04231K.
[27] S. Dutta, C. Rivetti, N.R. Gassman, C.G. Young, B.T. Jones, K. Scarpinato, M. Guthold, Analysis of single, cisplatin-induced DNA bends by atomic force microscopy and simulations, Journal of Molecular Recognition. 31 (2018) e2731. https://doi.org/10.1002/jmr.2731.
[28] B. Maity, Z. Li, K. Niwase, C. Ganser, T. Furuta, T. Uchihashi, D. Lu, T. Ueno, Single-molecule level dynamic observation of disassembly of the apo-ferritin cage in solution, Phys. Chem. Chem. Phys. 22 (2020) 18562–18572. https://doi.org/10.1039/D0CP02069A.
[29] S. Kumar, M.L. Cartron, N. Mullin, P. Qian, G.J. Leggett, C.N. Hunter, J.K. Hobbs, Direct Imaging of Protein Organization in an Intact Bacterial Organelle Using High-Resolution Atomic Force Microscopy, ACS Nano. 11 (2017) 126–133. https://doi.org/10.1021/acsnano.6b05647.
[30] D.M. Bangalore, I. Tessmer, Unique insight into protein-DNA interactions from single molecule atomic force microscopy, AIMS Biophysics. 5 (2018) 194. https://doi.org/10.3934/biophy.2018.3.194.

[31] Y.L. Lyubchenko, Direct AFM visualization of the nanoscale dynamics of biomolecular complexes, J. Phys. D: Appl. Phys. 51 (2018) 403001. https://doi.org/10.1088/1361-6463/aad898.
[32] M.V. Sukhanova, L. Hamon, M.M. Kutuzov, V. Joshi, S. Abrakhi, I. Dobra, P.A. Curmi, D. Pastre, O.I. Lavrik, A Single-Molecule Atomic Force Microscopy Study of PARP1 and PARP2 Recognition of Base Excision Repair DNA Intermediates, Journal of Molecular Biology. 431 (2019) 2655–2673. https://doi.org/10.1016/j.jmb.2019.05.028.
[33] M.T. Mawhinney, R. Liu, F. Lu, J. Maksimoska, K. Damico, R. Marmorstein, P.M. Lieberman, B. Urbanc, CTCF-Induced Circular DNA Complexes Observed by Atomic Force Microscopy, Journal of Molecular Biology. 430 (2018) 759–776. https://doi.org/10.1016/j.jmb.2018.01.012.
[34] D.M. Bangalore, H.S. Heil, C.F. Mehringer, L. Hirsch, K. Hemmen, K.G. Heinze, I. Tessmer, Automated AFM analysis of DNA bending reveals initial lesion sensing strategies of DNA glycosylases, Scientific Reports. 10 (2020) 15484. https://doi.org/10.1038/s41598-020-72102-7.
[35] P. Ghatak, K. Karmakar, S. Kasetty, D. Chatterji, Unveiling the Role of Dps in the Organization of Mycobacterial Nucleoid, PLOS ONE. 6 (2011) e16019. https://doi.org/10.1371/journal.pone.0016019.
[36] P. Ceci, A. Ilari, E. Falvo, L. Giangiacomo, E. Chiancone, Reassessment of Protein Stability, DNA Binding, and Protection of Mycobacterium smegmatis Dps, J. Biol. Chem. 280 (2005) 34776–34785. https://doi.org/10.1074/jbc.M502343200.
[37] S.P. Santos, E.P. Mitchell, H.G. Franquelim, M.A.R.B. Castanho, I.A. Abreu, C.V. Romão, Dps from Deinococcus radiodurans: oligomeric forms of Dps1 with distinct cellular functions and Dps2 involved in metal storage, The FEBS Journal. 282 (2015) 4307–4327. https://doi.org/10.1111/febs.13420.
[38] V.V. Melekhov, U.S. Shvyreva, A.A. Timchenko, M.N. Tutukina, E.V. Preobrazhenskaya, D.V. Burkova, V.G. Artiukhov, O.N. Ozoline, S.S. Antipov, Modes of Escherichia coli Dps Interaction with DNA as Revealed by Atomic Force Microscopy, PLOS ONE. 10 (2015) e0126504. https://doi.org/10.1371/journal.pone.0126504.
[39] N.A. Barinov, V.V. Prokhorov, E.V. Dubrovin, D.V. Klinov, AFM visualization at a single-molecule level of denaturated states of proteins on graphite, Colloids Surf. B Biointerfaces. 146 (2016) 777–784. https://doi.org/10.1016/j.colsurfb.2016.07.014.
[40] N.A. Barinov, A.D. Protopopova, E.V. Dubrovin, D.V. Klinov, Thermal denaturation of fibrinogen visualized by single-molecule atomic force microscopy, Colloids Surf. B Biointerfaces. 167 (2018) 370–376. https://doi.org/10.1016/j.colsurfb.2018.04.037.
[41] E.V. Dubrovin, N.A. Barinov, T.E. Schäffer, D.V. Klinov, In Situ Single-Molecule AFM Investigation of Surface-Induced Fibrinogen Unfolding on Graphite, Langmuir. 35 (2019) 9732–9739. https://doi.org/10.1021/acs.langmuir.9b01178.
[42] E.V. Dubrovin, D.V. Klinov, T.E. Schäffer, Evidence of (anti)metamorphic properties of modified graphitic surfaces obtained in real time at a single-molecule level, Colloids and Surfaces B: Biointerfaces. 193 (2020) 111077. https://doi.org/10.1016/j.colsurfb.2020.111077.
[43] M.A. Marko, R. Chipperfield, H.C. Birnboim, A procedure for the large-scale isolation of highly purified plasmid DNA using alkaline extraction and binding to glass powder, Analytical Biochemistry. 121 (1982) 382–387. https://doi.org/10.1016/0003-2697(82)90497-3.
[44] I. Yaminsky, A. Akhmetova, G. Meshkov, Femtoscan online software and visualization of nano-objecs in high-resolution microscopy, Nanoindustry. 11 (2018) 414–416. https://doi.org/10.22184/1993-8578.2018.11.6.414.416.
[45] A.P. Tolstova, E.V. Dubrovin, Influence of pixelization on height measurement in atomic force microscopy, Ultramicroscopy. 207 (2019) 112846. https://doi.org/10.1016/j.ultramic.2019.112846.
[46] A.T. Winzer, C. Kraft, S. Bhushan, V. Stepanenko, I. Tessmer, Correcting for AFM tip induced topography convolutions in protein-DNA samples, Ultramicroscopy. 121 (2012) 8–15. https://doi.org/10.1016/j.ultramic.2012.07.002.
[47] E.V. Dubrovin, S. Speller, I.V. Yaminsky, Statistical Analysis of Molecular Nanotemplate Driven DNA Adsorption on Graphite, Langmuir. 30 (2014) 15423–15432. https://doi.org/10.1021/la5041773.

[48] C.E. Blanchet, A. Spilotros, F. Schwemmer, M.A. Graewert, A. Kikhney, C.M. Jeffries, D. Franke, D. Mark, R. Zengerle, F. Cipriani, S. Fiedler, M. Roessle, D.I. Svergun, Versatile sample environments and automation for biological solution X-ray scattering experiments at the P12 beamline (PETRA III, DESY), J Appl Cryst. 48 (2015) 431–443. https://doi.org/10.1107/S160057671500254X.
[49] D.I. Svergun, Determination of the regularization parameter in indirect-transform methods using perceptual criteria, Journal of Applied Crystallography. 25 (1992) 495–503. https://doi.org/10.1107/S0021889892001663.
[50] D.I. Svergun, Restoring Low Resolution Structure of Biological Macromolecules from Solution Scattering Using Simulated Annealing, Biophysical Journal. 76 (1999) 2879–2886. https://doi.org/10.1016/S0006-3495(99)77443-6.
[51] M.V. Petoukhov, D. Franke, A.V. Shkumatov, G. Tria, A.G. Kikhney, M. Gajda, C. Gorba, H.D.T. Mertens, P.V. Konarev, D.I. Svergun, New developments in the ATSAS program package for small-angle scattering data analysis, J Appl Cryst. 45 (2012) 342–350. https://doi.org/10.1107/S0021889812007662.
[52] D. Svergun, C. Barberato, M.H.J. Koch, CRYSOL– a Program to Evaluate X-ray Solution Scattering of Biological Macromolecules from Atomic Coordinates, Journal of Applied Crystallography. 28 (1995) 768–773. https://doi.org/10.1107/S0021889895007047.
[53] P. Bernadó, E. Mylonas, M.V. Petoukhov, M. Blackledge, D.I. Svergun, Structural Characterization of Flexible Proteins Using Small-Angle X-ray Scattering, J. Am. Chem. Soc. 129 (2007) 5656–5664. https://doi.org/10.1021/ja069124n.
[54] G. Tria, H.D.T. Mertens, M. Kachala, D.I. Svergun, Advanced ensemble modelling of flexible macromolecules using X-ray solution scattering, IUCrJ. 2 (2015) 207–217. https://doi.org/10.1107/S205225251500202X.
[55] M.B. Kozin, D.I. Svergun, Automated matching of high- and low-resolution structural models, Journal of Applied Crystallography. 34 (2001) 33–41. https://doi.org/10.1107/S0021889800014126.
[56] E.Yu. Soshinskaya, L.A. Dadinova, A.A. Mozhaev, E.V. Shtykova, Effect of Buffer Composition on Conformational Flexibility of N-Terminal Fragments of Dps and the Nature of Interactions with DNA. Small-Angle X-Ray Scattering Study, Crystallogr. Rep. 65 (2020) 891–899. https://doi.org/10.1134/S1063774520060334.
[57] E.V. Dubrovin, M. Schächtele, D.V. Klinov, T.E. Schäffer, Time-Lapse Single-Biomolecule Atomic Force Microscopy Investigation on Modified Graphite in Solution, Langmuir. 33 (2017) 10027–10034. https://doi.org/10.1021/acs.langmuir.7b02220.
[58] N.A. Barinov, I.I. Vlasova, A.V. Sokolov, V.A. Kostevich, E.V. Dubrovin, D.V. Klinov, High-resolution atomic force microscopy visualization of metalloproteins and their complexes, Biochimica et Biophysica Acta (BBA) - General Subjects. 1862 (2018) 2862–2868. https://doi.org/10.1016/j.bbagen.2018.09.008.
[59] D.V. Klinov, A.D. Protopopova, D.S. Andrianov, R.I. Litvinov, J.W. Weisel, An Improved Substrate for Superior Imaging of Individual Biomacromolecules with Atomic Force Microscopy, Colloids and Surfaces B: Biointerfaces. 196 (2020) 111321. https://doi.org/10.1016/j.colsurfb.2020.111321.
[60] S. Kasas, G. Dietler, DNA-protein interactions explored by atomic force microscopy, Semin. Cell Dev. Biol. 73 (2018) 231–239. https://doi.org/10.1016/j.semcdb.2017.07.015.
[61] S. Santos, V. Barcons, H.K. Christenson, J. Font, N.H. Thomson, The Intrinsic Resolution Limit in the Atomic Force Microscope: Implications for Heights of Nano-Scale Features, PLOS ONE. 6 (2011) e23821. https://doi.org/10.1371/journal.pone.0023821.
[62] Y. Zhang, B.P. Orner, Self-Assembly in the Ferritin Nano-Cage Protein Superfamily, International Journal of Molecular Sciences. 12 (2011) 5406–5421. https://doi.org/10.3390/ijms12085406.
[63] J. Adamcik, J.-H. Jeon, K.J. Karczewski, R. Metzler, G. Dietler, Quantifying supercoiling-induced denaturation bubbles in DNA, Soft Matter. 8 (2012) 8651–8658. https://doi.org/10.1039/C2SM26089A.
[64] O.N. Koroleva, E.V. Dubrovin, I.V. Yaminsky, V.L. Drutsa, Effect of DNA bending on transcriptional interference in the systems of closely spaced convergent promoters, Biochimica et Biophysica Acta (BBA) - General Subjects. 1860 (2016) 2086–2096. https://doi.org/10.1016/j.bbagen.2016.06.026.

[65] A.R. Cutter, J.J. Hayes, A brief review of nucleosome structure, FEBS Letters. 589 (2015) 2914–2922. https://doi.org/10.1016/j.febslet.2015.05.016.
[66] E.C. Beckwitt, M. Kong, B. Van Houten, Studying protein-DNA interactions using atomic force microscopy, Seminars in Cell & Developmental Biology. 73 (2018) 220–230. https://doi.org/10.1016/j.semcdb.2017.06.028.
[67] A. Vologodskii, M. D. Frank-Kamenetskii, Strong bending of the DNA double helix, Nucleic Acids Research. 41 (2013) 6785–6792. https://doi.org/10.1093/nar/gkt396.